Journal of *Marine Science and Engineering*

MDPI

Article

Kinematic Calibration for the 3-UPS/S Shipborne Stabilized Platform Based on Transfer Learning

Min Xu [1], Wenjie Tian [1,*] and Xiangpeng Zhang [2]

[1] School of Marine Science and Technology, Tianjin University, Tianjin 300072, China; xumin_1101@tju.edu.cn
[2] Key Laboratory of Mechanism Theory and Equipment Design of Ministry of Education, Tianjin University, Tianjin 300072, China; xiangpengzhang@tju.edu.cn
* Correspondence: wenjietian@tju.edu.cn

Abstract: The three-degrees-of-freedom (3-DOF) parallel robot is commonly employed as a shipborne stabilized platform for real-time compensation of ship disturbances. Pose accuracy is one of its most critical performance indicators. Currently, neural networks have been applied to the kinematic calibration of stabilized platforms to compensate for pose errors and enhance motion accuracy. However, collecting a large amount of measured configuration data for robots entails high costs and time, which restricts the widespread use of neural networks. In this study, a "transfer network" is established by combining fine-tuning with a Back Propagation (BP) neural network. This network takes the motion transmission characteristics inherent in the ideal kinematic model as prior knowledge and transfers them to a network trained based on the actual poses. Compared with the conventional BP neural network trained by actual poses alone, the transfer network shows significant performance advantages, effectively solving the problems of low prediction accuracy and weak generalization ability in the case of small-sample measured data. Considering this, the impact pattern of the sample number of the actual pose on the effectiveness of transfer learning is revealed through the construction of multiple transfer network models under varying sample numbers of the actual pose, providing valuable marine engineering guidance. Finally, simulated sea-service experiments were conducted on the 3-UPS/S shipborne stabilized platform to validate the correctness and superiority of the proposed method.

Keywords: shipborne stabilized platform; kinematic calibration; transfer learning; BP neural network; parallel robot; ocean engineering

Citation: Xu, M.; Tian, W.; Zhang, X. Kinematic Calibration for the 3-UPS/S Shipborne Stabilized Platform Based on Transfer Learning. *J. Mar. Sci. Eng.* **2024**, *12*, 275. https://doi.org/10.3390/jmse12020275

Academic Editor: Sergei Chernyi

Received: 10 January 2024
Revised: 26 January 2024
Accepted: 31 January 2024
Published: 2 February 2024

1. Introduction

In maritime environments, vessels are subject to disturbances from wind, waves, currents, and other oceanic factors, resulting in 6-DOF motion. For oceanographic research vessels engaged in marine observation missions with scientific instruments, the 3-DOF motion—roll, pitch, and yaw—leads to attitude variations that significantly impact the measurement accuracy of the scientific instruments. Utilizing a 3-DOF robot as a shipborne attitude-stabilized platform to compensate for the vessel's attitude changes in real-time is considered an effective engineering solution [1].

Due to the advantages of parallel robots in terms of payload capacity, stiffness, and response speed [2], they are well-suited for carrying instruments and equipment on ships, compensating for the dynamic changes in their attitude. Whether the shipborne stabilized platform can effectively compensate for the impact of vessel motion on onboard equipment depends, on the one hand, on the stability control of the stabilized platform. However, for high-precision compensation, the inherent accuracy of the stabilized platform itself is also a crucial factor affecting the compensation results. Therefore, conducting kinematic calibration for the stabilized platform to compensate for end-effector errors is of significant importance in improving the motion accuracy of the stabilized platform [3].

The sources of errors affecting the accuracy of parallel robots include geometric errors and non-geometric errors [4,5]. Geometric errors can often be calibrated using traditional kinematic calibration methods based on error models. The calibration process includes error modeling, error measurement, parameter identification, and error compensation. Extensive research using this method has been conducted [6–8]. Although traditional kinematic calibration methods have the advantages of fast convergence and clear physical interpretation, the process of modeling and parameter identification is complex. Moreover, they neglect the influence of non-geometric error factors. Therefore, some scholars [9–11] have investigated new error models that include non-geometric errors for calibration. However, due to the highly nonlinear and strongly coupled nature of non-geometric error parameters, error modeling and calibration methods tailored to individual types of non-geometric error sources lack general theoretical guidance.

In response to these limitations, model-free calibration methods have been proposed. Among these methods, neural networks are the most widely used. When there are abundant measured configuration data available, neural networks can construct a nonlinear mapping model between robot nominal joint variables and end-effector pose errors without relying on the kinematic model [12,13]. Gao et al. [14] proposed an articulated arm coordinate measuring machine (AACMM) modeling and error compensation method based on BP neural networks. They formulated data acquisition strategies based on the actual measurement behavior of joint space and achieved a 97% reduction in AACMM error after compensation. Nguyen et al. [15] combined the model-based extended Kalman filter (EKF) algorithm with neural network-based calibration techniques and demonstrated the effectiveness of the method in calibrating errors from all error sources through simulations and experiments on serial PUMA and HH800 manipulators. Yu et al. [16] presented a hybrid neural network calibration method that combines the output of the BP neural network and the radical basis function (RBF) neural network and verified its correctness through experiments on a 6-DOF parallel robot. Wang et al. [17] used the product of exponentials (POE) method as the foundation and further compensated for non-geometric errors through a multi-layer perceptron neural network (MLPNN) optimized by the beetle swarm optimization algorithm, achieving efficient calibration of the SIASUN SR210D robot manipulator. Maghami et al. [18] proposed a two-step calibration method based on artificial neural networks (ANNs) for a master-slave cooperative robot system. By training two ANN models to compensate for master-slave relative errors and master robot errors, the absolute accuracy of the master robot and relative tracking precision are improved.

It can be observed that the application of neural networks is increasingly pervasive, and the utilization methods have diversified. However, the training of neural network models is based on a large amount of data to explore the underlying patterns in the data. Therefore, their accuracy heavily relies on the training dataset's quality and quantity [19]. In previous studies, the establishment of predictive models for actual poses was based on many measured configuration data. However, acquiring a large number of data samples entails substantial costs in terms of both time and financial resources. Even with sufficient measured data, data preprocessing and network structure optimization can also affect the timeliness of the calibration. All these factors make existing calibration methods inadequate to meet the urgent need for high-efficient and low-cost calibration of shipborne stabilized platforms in marine engineering applications.

Transfer learning is a branch of machine learning that focuses on achieving knowledge transfer across domains to enhance the performance of network learning or reduce the required amount of data. The core idea of transfer learning is [20]: given a source domain $\mathcal{D}_S$ with abundant data and target domain $\mathcal{D}_T$ with limited data, source learning task $\mathcal{T}_S$, and target learning task $\mathcal{T}_T$, transfer learning aims at helping enhance learning ability of the target prediction function $f_T(\cdot)$ in $\mathcal{T}_T$, based on the knowledge in $\mathcal{D}_S$ and $\mathcal{T}_S$, where $\mathcal{D}_S \neq \mathcal{D}_T$ and/or $\mathcal{T}_S \neq \mathcal{T}_T$. However, transfer learning typically requires a certain degree of correlation between the two domains to ensure the transferred knowledge is effective [21]. This concept is similar to human learning, where acquiring one skill can make it relatively

easier to learn another related skill. Transfer learning is typically combined with convolutional neural networks (CNNs), BP neural networks, and other architectures to enhance the classification or prediction capabilities of neural networks, making it a hot topic in research. It has demonstrated excellent results in various fields such as computer vision, fault diagnosis, and natural language processing [22–24]. Despite these successes, transfer learning methods have not yet been introduced to the field of robot kinematic calibration. The kinematic model of a real robot system with errors exhibits a high similarity to the ideal kinematic model. Therefore, an effort is made to regard the motion transmission characteristics inherent in the ideal kinematic model as prior knowledge and transfer them to a network trained based on actual pose data. This approach holds the potential to address the challenges of low prediction accuracy when approximating small-sample measured datasets.

This study investigates a transfer learning-based kinematic calibration method for a shipborne stabilized platform to address the issue of low network prediction accuracy and weak generalization capabilities due to insufficient measured data. In Section 2, relevant theoretical knowledge about the 3-UPS/S shipborne stabilized platform is introduced. In Section 3, the transfer network for predicting actual poses is established by combining fine-tuning with a BP neural network, with fitting simulated desired poses as the source task and actual poses as the target task. Its performance is compared with that of a conventional BP neural network trained by actual pose data alone, demonstrating its superior performance. On this basis, the impact pattern of the sample number of the actual pose on the effectiveness of transfer learning is investigated and revealed, providing valuable ocean engineering guidance. In Section 4, focusing on the maritime application scenario of the shipborne stabilized platform, error compensation experiments are conducted to validate the proposed method's effectiveness. Section 5 presents the conclusions.

The theoretical and engineering value of this research lies in the following:

- When using the same small sample number, the transfer network will effectively solve the problems of inadequate prediction accuracy and weak generalization ability.
- When the same prediction accuracy is reached, the sample number required by the transfer network will be smaller, contributing to higher efficiency and lower costs.
- In ocean engineering, the obtained impact pattern is capable of providing reference recommendations on the optimal choice of calibration method (i.e., the type of predictive network), thereby maximizing calibration efficiency.

2. 3-UPS/S Shipborne Stabilized Platform

In this section, the research object of this paper is first introduced, i.e., the 3-UPS/S parallel shipborne stabilized platform. Then, the pose description and inverse displacement kinematics analysis are carried out, which is a necessary preparation for generating and preprocessing the dataset required for training neural networks.

2.1. System Description

The structure of the 3-UPS/S parallel stabilized platform is shown in Figure 1. It consists of a moving platform, a fixed base, three UPS limbs, and a central constraint limb. Each UPS limb connects to the moving platform through a spherical joint (S joint) and to the fixed base through a universal joint (U joint). The central constraint limb connects to the moving platform through an S joint and is fixedly connected to the fixed base. The three translational DOF motions of the moving platform are restricted by the central constraint limb, while the three rotational DOF motions can be achieved by controlling three UPS limb length variations.

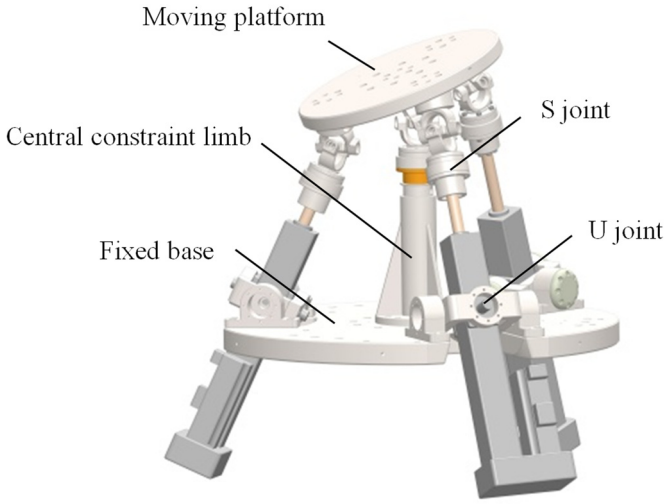

Figure 1. The 3-UPS/S parallel stabilized platform structure.

2.2. Establishment of the Coordinate System and Pose Description

As shown in Figure 2, A_i and B_i ($i = 1, 2, 3$) represent the centers of the U joints and S joints in the ith UPS limb, forming equilateral triangles $\Delta A_1A_2A_3$ and $\Delta B_1B_2B_3$, respectively. A represents the intersection of the central constraint limb with $\Delta A_1A_2A_3$, and coincides with the geometric center of $\Delta A_1A_2A_3$. B represents the center of the S joint on the top of the central constraint limb, coinciding with the geometric center of $\Delta B_1B_2B_3$. The axis of the central constraint limb is perpendicular to $\Delta A_1A_2A_3$. Reference frame A-xyz is established at A, the x-axis passes through A_1, the z-axis is perpendicular to $\Delta A_1A_2A_3$, and the y-axis satisfies the right-hand rule. To describe the pose of the moving platform, body-fixed frame B-uvw is established at B, the u-axis passes through B_1, the w-axis is perpendicular to $\Delta B_1B_2B_3$, and the v-axis satisfies the right-hand rule. $\phi_i = 2(i-1)\pi/3$ is the distribution angle of A_i and B_i within their respective planes. The circumscribed circle radii of $\Delta A_1A_2A_3$ and $\Delta B_1B_2B_3$ are denoted as a and b, respectively, and the height of the central constraint limb is denoted as h.

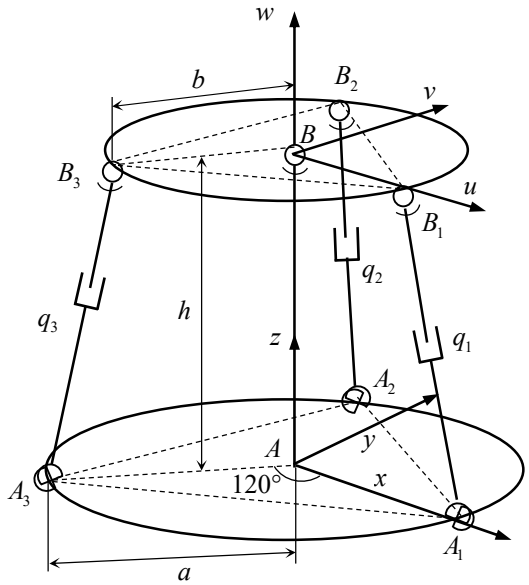

Figure 2. The coordinate system of the 3-UPS/S parallel stabilized platform.

The orientation matrix $\boldsymbol{R}_B^A$ of frame B-uvw with respect to frame A-xyz can be described as

$$\boldsymbol{R}_B^A = \begin{bmatrix} c\alpha c\gamma - c\beta s\alpha s\gamma & -c\beta c\gamma s\alpha - s\gamma c\alpha & s\alpha s\beta \\ c\gamma s\alpha + c\alpha c\beta s\gamma & c\alpha c\beta c\gamma - s\alpha s\gamma & -c\alpha s\beta \\ s\beta s\gamma & c\gamma s\beta & c\beta \end{bmatrix} \tag{1}$$

where α represents the azimuth angle, β represents the tilt angle, and γ represents the twist angle.

2.3. Inverse Displacement Kinematics Analysis

Given the known pose of the moving platform, the actuated joint variables can be obtained from

$$q_i = \left\| \overrightarrow{A_i B_i} \right\| = \left\| h\boldsymbol{k} + \boldsymbol{R}_B^A \boldsymbol{b}_i - \boldsymbol{a}_i \right\|, \ i = 1, 2, 3 \tag{2}$$

where $\boldsymbol{k}$ is the unit vector along the z-axis, $\boldsymbol{R}_B^A$ is the orientation matrix, $\boldsymbol{a}_i$ and $\boldsymbol{b}_i$ represent the position vectors of A_i and B_i measured in the frames A-xyz and B-uvw, respectively. Specifically,

$$\boldsymbol{a}_i = \begin{pmatrix} a\cos\phi_i \\ a\sin\phi_i \\ 0 \end{pmatrix}, \ \boldsymbol{b}_i = \begin{pmatrix} b\cos\phi_i \\ b\sin\phi_i \\ 0 \end{pmatrix}, \ \boldsymbol{k} = \begin{pmatrix} 0 \\ 0 \\ 1 \end{pmatrix} \tag{3}$$

where $\phi_i = 2(i-1)\pi/3$ $(i = 1, 2, 3)$.

3. Methods of Transfer Learning

In ocean engineering, acquiring a large amount of actual pose data is complex and costly, presenting a challenge when using data-driven neural networks to solve the kinematic calibration problem of shipborne stabilized platforms. To address this issue, simulation studies are conducted in this section with the 3-UPS/S shipborne stabilized platform introduced in the previous section as the research object. Based on transfer learning theories, a transferred network for predicting the actual poses is established using the desired pose data obtained from kinematic models as prior knowledge. Furthermore, the relationship between the transfer learning effectiveness and the sample number of the actual pose is investigated to reveal the influence pattern.

3.1. Motivation

According to the theory of transfer learning, there should be differences as well as correlations between the source domain data and the target domain data. The strength of these correlations affects the effectiveness of transfer learning [21]. For robot systems, similar relationships exist between the desired and actual poses in their workspace. That is, macro-level motions are comparable, while micro-level errors differ. During the calibration process, measuring a large amount of actual pose data is challenging, while ideal pose data can be generated in abundance using kinematic models. Therefore, in this study, "building a mapping model from nominal actuated joint variables to desired end-effector poses" is taken as the source task and "building a mapping model from nominal actuated joint variables to actual end-effector poses" as the target task. According to this transfer learning strategy, the theory of accurately predicting actual end-effector poses under the condition of limited measured data is explored, which provides new technological insights for improving the calibration efficiency of shipborne stabilized platforms. Figure 3 shows the learning process of transfer learning.

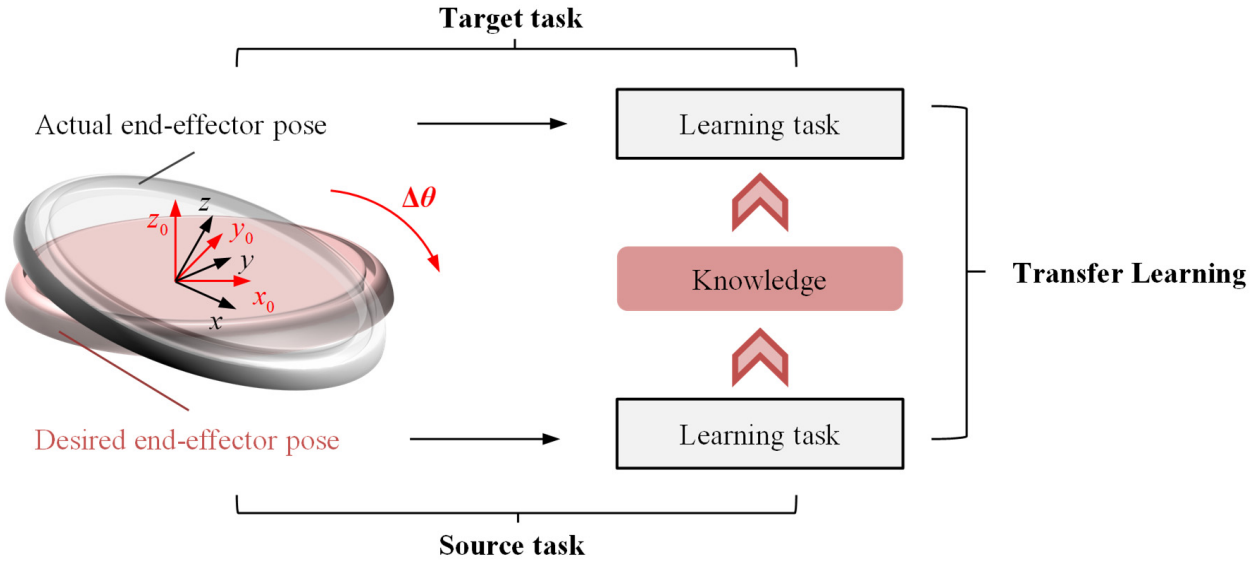

Figure 3. Learning process of transfer learning.

3.2. Transfer Scheme

Currently, fine-tuning [25] is one of the most widely used approaches in the field of neural network transfer learning. The core idea of this approach is to apply the knowledge obtained from the source task in the form of trained parameters to the target task. Training the target domain model only requires fine-tuning these parameters. Since the parameters of the target domain network are in a relatively good position from the beginning of fine-tuning, this approach not only saves a lot of computational resources and time but often leads to better results compared to training directly with target domain data. In this study, a fine-tuning approach based on the BP neural network is adopted to predict actual poses.

The BP neural network [26] is composed of an input layer, hidden layers, and an output layer. Its forward propagation process can be represented as

$$\boldsymbol{o}^l = f_l\left(\mathbf{W}^l \cdot \boldsymbol{o}^{l-1} + \boldsymbol{b}^l\right) \tag{4}$$

where $\boldsymbol{o}^l$ and $\boldsymbol{o}^{l-1}$ represent the outputs of layers l and $l-1$, respectively, $\mathbf{W}^l$ is the weight of layer l, $\boldsymbol{b}^l$ is the bias of layer l, and $f_l(\cdot)$ denotes the activation function. In this study, with three neural network inputs and outputs, a four-layer network structure is considered. When applied to the task of predicting actual poses, the target domain fitting function can be approximated by the BP neural network as follows:

$$\boldsymbol{\theta} = f_3\left(\mathbf{W}^3 f_2\left(\mathbf{W}^2 f_1\left(\mathbf{W}^1 \boldsymbol{q} + \boldsymbol{b}^1\right) + \boldsymbol{b}^2\right) + \boldsymbol{b}^3\right) \tag{5}$$

where nominal actuated joint variable $\boldsymbol{q} = \begin{pmatrix} q_1 \\ q_2 \\ q_3 \end{pmatrix}$ is the input vector, and the actual end-effector pose $\boldsymbol{\theta} = \begin{pmatrix} \alpha \\ \beta \\ \gamma \end{pmatrix}$ is the output vector.

The source domain fitting function can be approximated by the BP neural network as follows:

$$\boldsymbol{\theta}_0 = f_3\left(\mathbf{W}_0^3 f_2\left(\mathbf{W}_0^2 f_1\left(\mathbf{W}_0^1 \boldsymbol{q} + \boldsymbol{b}_0^1\right) + \boldsymbol{b}_0^2\right) + \boldsymbol{b}_0^3\right) \tag{6}$$

where nominal actuated joint variable $\boldsymbol{q} = \begin{pmatrix} q_1 \\ q_2 \\ q_3 \end{pmatrix}$ is the input vector, and the desired end-effector pose $\boldsymbol{\theta}_0 = \begin{pmatrix} \alpha_0 \\ \beta_0 \\ \gamma_0 \end{pmatrix}$ is the output vector. The pre-trained parameters $\mathbf{W}_0^i$ and $\boldsymbol{b}_0^i$ are extracted and transferred, serving as the initial values for the target domain network parameters $\mathbf{W}^i$ and $\boldsymbol{b}^i$ $(i = 1, 2, 3)$. Subsequently, the target domain network is further trained using actual poses. The neural network, trained using this approach, is referred to as a "transfer network" in this study. Its comparative group is a conventional BP neural network, which is initialized with random weights and biases and trained only using actual poses. The establishment schemes of the two neural networks are shown in Figure 4.

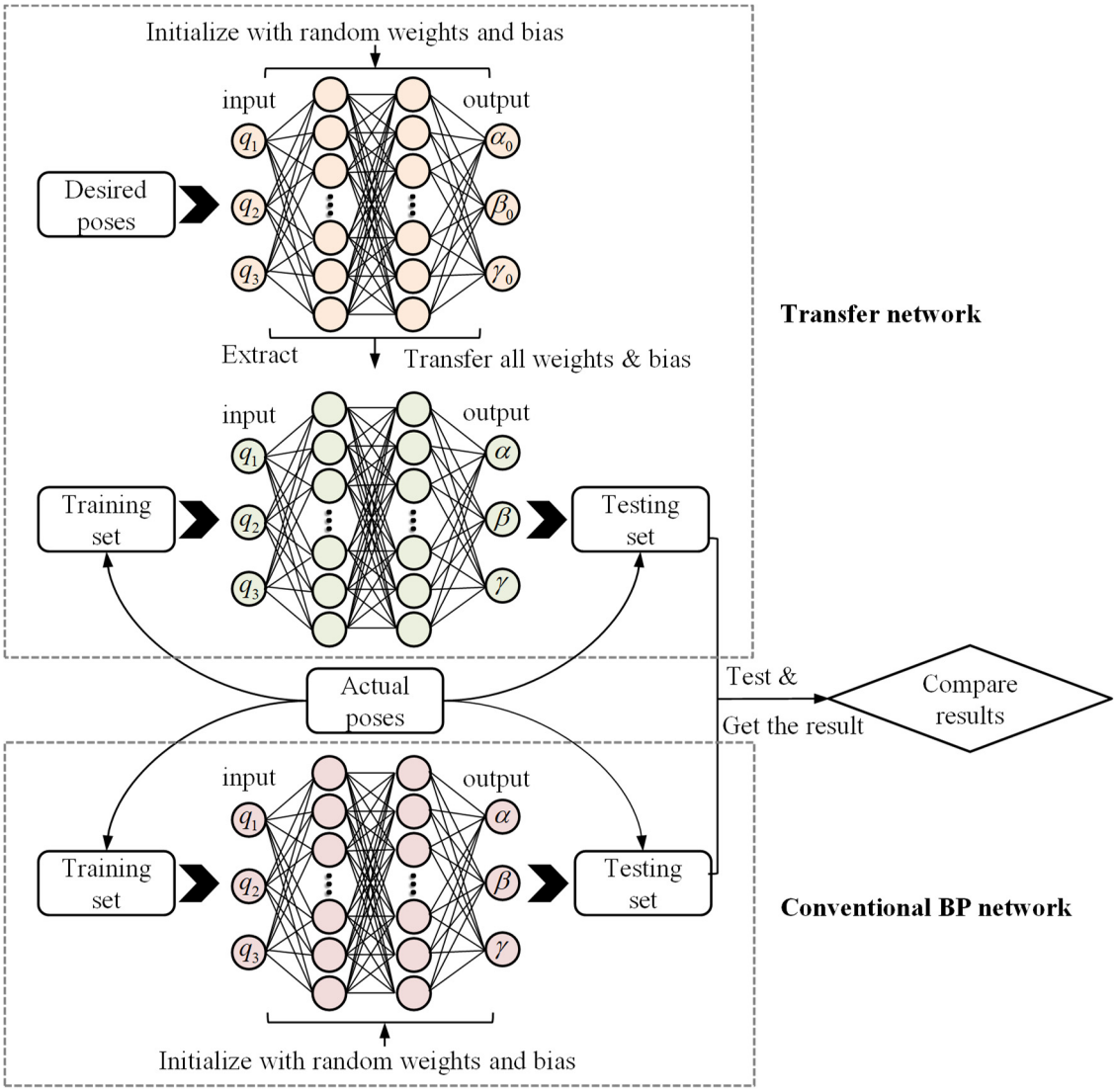

Figure 4. Establishment schemes of the transfer network and the conventional BP network.

3.3. Evaluation Index

This paper utilizes both the transfer network and the conventional BP neural network to predict the actual poses separately. To quantitatively evaluate the similarity between the actual pose $\boldsymbol{\theta}$ and its predicted value $\hat{\boldsymbol{\theta}}$, the pose error calculation formula is presented first. The desired and actual orientation matrices are denoted as $\boldsymbol{R}_1$ and $\boldsymbol{R}_2$, respectively. Based

on the premise that the orientation error is small, the orientation error matrix $\Delta \boldsymbol{R}$ can be written as [27]

$$\Delta \boldsymbol{R} = \boldsymbol{R}_1^{-1} \boldsymbol{R}_2 = \begin{bmatrix} e_{11} & e_{12} & e_{13} \\ e_{21} & e_{22} & e_{23} \\ e_{31} & e_{32} & e_{33} \end{bmatrix} \tag{7}$$

From Equation (7), the orientation errors of the moving platform can be obtained.

$$\Delta \boldsymbol{\theta} = \begin{pmatrix} \Delta\alpha \\ \Delta\beta \\ \Delta\gamma \end{pmatrix} = \frac{1}{2} \begin{pmatrix} e_{32} - e_{23} \\ e_{13} - e_{31} \\ e_{21} - e_{12} \end{pmatrix} \tag{8}$$

Based on the obtained orientation errors, accuracy evaluation indices are defined for each configuration from both an overall perspective and accuracy in each individual orientation direction.

Evaluation index 1: According to ISO 230-1 [28], the orientation volumetric error $\|\Delta\boldsymbol{\theta}\|$ of the end-effector is used to measure the difference between the actual pose $\boldsymbol{\theta}$ and its predicted value $\hat{\boldsymbol{\theta}}$. A smaller $\|\Delta\boldsymbol{\theta}\|$ indicates better prediction performance.

$$\|\Delta\boldsymbol{\theta}\| = \sqrt{\Delta\alpha^2 + \Delta\beta^2 + \Delta\gamma^2} \tag{9}$$

Evaluation index 2: The orientation errors $\|\Delta\alpha\|$, $\|\Delta\beta\|$, $\|\Delta\gamma\|$ for each individual orientation direction are defined to measure the differences between the actual poses α, β, γ and their predicted values $\hat{\alpha}$, $\hat{\beta}$, $\hat{\gamma}$, respectively, for rotations around the x, y, and z axes. Smaller values of $\|\Delta\alpha\|$, $\|\Delta\beta\|$, $\|\Delta\gamma\|$ indicate a better prediction performance.

$$\|\Delta\alpha\| = \sqrt{\Delta\alpha^2},\ \|\Delta\beta\| = \sqrt{\Delta\beta^2},\ \|\Delta\gamma\| = \sqrt{\Delta\gamma^2} \tag{10}$$

3.4. Implementation of Transfer Learning

3.4.1. Simulation Process

The simulation process for establishing the transfer network can be divided into the following steps:

- Step 1: Select source domain configurations. The rotational angle ranges of the moving platform around the x, y, and z axes are -20° to 20°, -20° to 20°, and -10° to 10°, respectively. Considering the typical scenario in transfer learning, where the source domain often has a much larger sample size than the target domain, 1331 desired end-effector poses within the workspace are uniformly selected as the source domain configurations (as shown in Figure 5a).
- Step 2: Select target domain configurations. According to the method described in reference [29], a full-parameter geometric error model for the 3-UPS/S mechanism is established. The error source parameters identified through the preliminary geometric identification method are assigned to each error source. The error model is then used to generate end-effector pose errors. Superimposing these end-effector pose errors onto 150 uniformly selected configurations (as shown in Figure 5b) and adding Gaussian noise with a standard deviation of 2 μm to simulate measurement noise according to the method mentioned in ISO-9283 [30] yields 150 actual end-effector poses for simulation.
- Step 3: Obtain the source domain and target domain datasets. For the selected two types of configurations, nominal actuated joint variables are calculated by substituting into Equation (2) and used as inputs for both the source and target networks. The desired poses and the actual poses obtained in steps 1 and 2 are taken as the outputs of the source and target networks, respectively.
- Step 4: A four-layer BP neural network is established and randomly initialized. Pre-training is performed using 1331 source domain samples.

- Step 5: The weights and biases, trained by the pre-training network, are all extracted and transferred as the initial value for the target network. Subsequently, the target network is further trained using target domain samples, randomly selecting 80% for training and the remaining 20% for testing.
- Step 6: The predictive accuracy is assessed by the testing set.

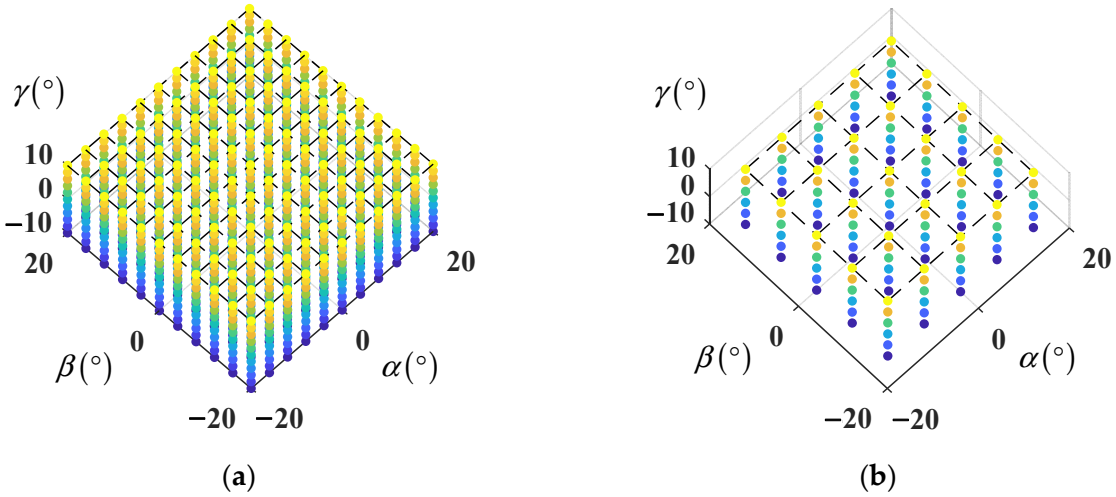

Figure 5. Configuration selection schemes. (**a**) 1331 configurations used to generate data for the source domain; (**b**) 150 configurations used to generate data for the target domain.

The simulation process of the conventional BP neural network is simpler compared to the transfer network, as it only trains the initial network structure using target domain samples. During the training process, the BP neural network and the transfer network have the same hidden layer node numbers, training algorithms, epoch limits, and other parameters. This parameter setup ensures that any differences in network training results are attributed to whether pre-training was conducted or not, rather than variations in parameters. As a result, the effectiveness of the proposed shipborne stabilized platform calibration method based on transfer learning can be accurately evaluated.

3.4.2. Simulation Results and Discussion

Following the simulated process described in the preceding section, the transfer network and BP network are separately trained. Subsequently, their performances are evaluated using defined evaluation indices. Based on the simulation results, the impact of transfer learning methods on the prediction ability of the network is validated. The performance comparisons of the two models on the training and testing configurations are shown in Figures 6 and 7, respectively.

It can be observed that using either the BP network or the transfer network for predictions, the error evaluation indices after calibration are both smaller than those before. However, in terms of the comparison of calibration accuracy between the two networks, whether in training or testing configurations, the transfer network proposed in this paper demonstrates a more precise prediction compared to the BP network. On our more focused testing configurations, after prediction with the transfer network, the mean orientation errors for three orientation directions $\|\Delta\alpha\|$, $\|\Delta\beta\|$, $\|\Delta\gamma\|$ and the mean orientation volumetric error $\|\Delta\boldsymbol{\theta}\|$ decreased from 0.177°, 0.047°, 0.051°, and 0.195° before calibration to 0.005°, 0.007°, 0.010°, and 0.015° after calibration. In contrast, when using the BP network for prediction, these indices only decreased to 0.021°, 0.018°, 0.024°, and 0.040°, respectively. Moreover, the maximums and standard deviations of the evaluation indices obtained by the transfer network are significantly smaller than those of the BP network (see Tables 1 and 2 for details). It can be judged that the transfer network exhibits stronger generalization capabilities, enabling the model to better cope with variations and complexities in the target domain. Even with limited measured

configuration data, the transfer network achieves great and stable prediction performance, demonstrating the superiority of applying this method to kinematic calibration on shipborne stabilized platforms.

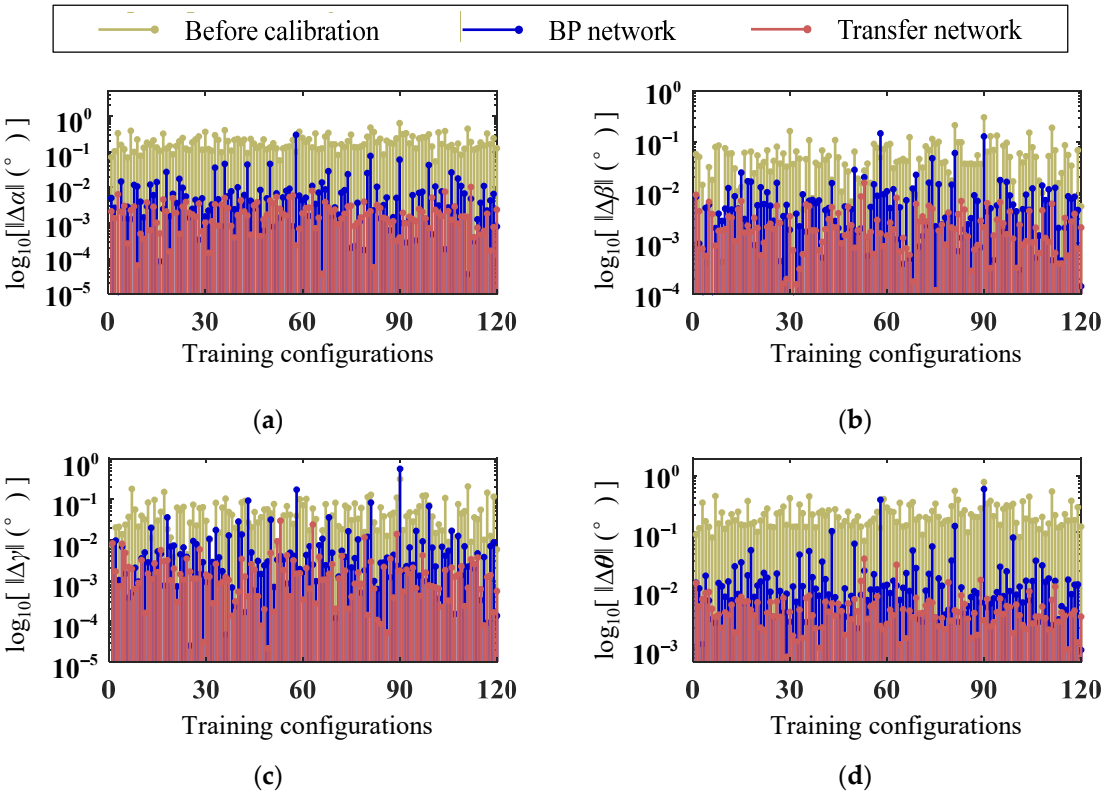

Figure 6. Performance comparison of the transfer network and the BP network on the training configurations. (**a**) In the direction of rotation around the *x*-axis; (**b**) in the direction of rotation around the *y*-axis; (**c**) in the direction of rotation around the *z*-axis; (**d**) overall accuracy.

Table 1. Simulated comparison of orientation errors for each individual orientation direction on testing configurations.

	Before Calibration			**BP Network**			**Transfer Network**		
	$\|\|\Delta\alpha\|\|$	$\|\|\Delta\beta\|\|$	$\|\|\Delta\gamma\|\|$	$\|\|\Delta\alpha\|\|$	$\|\|\Delta\beta\|\|$	$\|\|\Delta\gamma\|\|$	$\|\|\Delta\alpha\|\|$	$\|\|\Delta\beta\|\|$	$\|\|\Delta\gamma\|\|$
Mean (°)	0.177	0.047	0.051	0.021	0.018	0.024	0.005	0.007	0.010
Maximum (°)	0.421	0.144	0.196	0.112	0.067	0.089	0.024	0.042	0.049
SD (°)	0.093	0.038	0.043	0.024	0.016	0.021	0.005	0.009	0.011

Table 2. Simulated comparison of orientation volumetric error $\|\|\Delta\theta\|\|$ on testing configurations.

	Before Calibration	**BP Network**	**Transfer Network**
Mean (°)	0.195	0.040	0.015
Maximum (°)	0.479	0.136	0.055
SD (°)	0.099	0.031	0.014

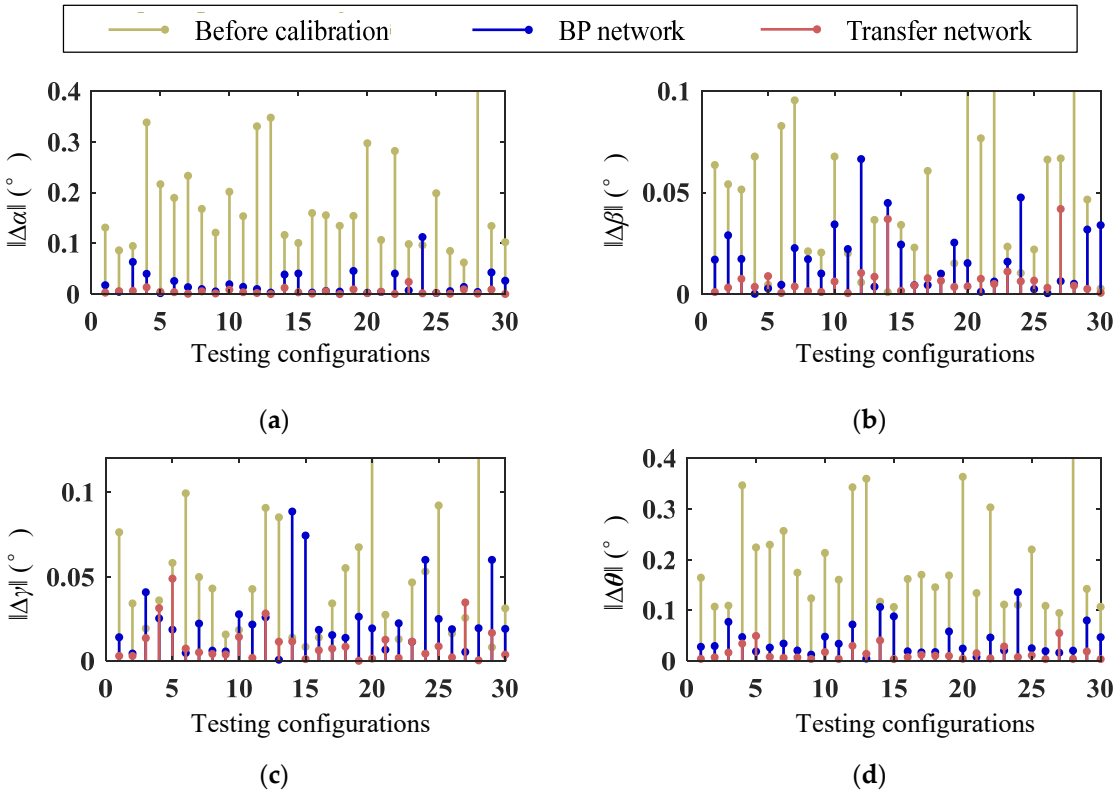

Figure 7. Performance comparison of the transfer network and the BP network on the testing configurations. (**a**) In the direction of rotation around the *x*-axis; (**b**) in the direction of rotation around the *y*-axis; (**c**) in the direction of rotation around the *z*-axis; (**d**) overall accuracy.

Finally, the end-effector pose $\hat{\boldsymbol{\theta}}$ predicted using the transfer network is utilized for error compensation. Error compensation serves as the last step in kinematic calibration. The inverse displacement kinematics of $\hat{\boldsymbol{\theta}}$ is performed to obtain $\hat{\boldsymbol{q}}$, which is then assigned to $\boldsymbol{q}$ in the control system. This correction of actuated joint variables serves to compensate for the end-effector pose error, aiming to bring the shipborne stabilized platform closer to the desired pose.

3.5. Relationship between Transfer Learning and the Sample Number of the Actual Pose

3.5.1. Simulation Process

Considering that the amount of target domain data is one of the key factors in the selection of transfer learning methods [31], this section further explores how different sample numbers of the actual pose affect the effectiveness of transfer learning based on the previous section (with 150 actual pose samples). The simulation strategy is to establish the transfer network and the BP network under different sample numbers of the actual pose, respectively. The simulation steps for establishing the transfer network are as follows:

- Step 1: Select source domain configurations. The selection of source domain configurations is the same as step 1 in Section 3.4.1, i.e., 1331 configurations as shown in Figure 5a.
- Step 2: Select target domain configurations. To account for variations in the sample number of the actual pose, the number of selected configurations in the target domain is appropriately increased here to establish a broader research range for the sample size. Consequently, 216 configurations are uniformly selected in the workspace (as shown in Figure 8). Following the methodology outlined in step 2 of Section 3.4.1, the corresponding 216 end-effector actual poses are obtained for simulation purposes.
- Step 3: Obtain the source domain and target domain datasets. For the selected two types of configurations, nominal actuated joint variables are calculated by substituting

them into Equation (2) and used as inputs for both the source and target networks. The desired poses and the actual poses obtained in steps 1 and 2 are taken as the outputs of the source and target networks, respectively.

- Step 4: A four-layer BP neural network is established and randomly initialized. Pre-training is performed using 1331 source domain samples.
- Step 5: "n" samples are selected from a total of 216 samples to construct the training set and testing set, with 80% for training and 20% for testing.
- Step 6: The weights and biases, trained by the pre-training network, are all extracted and transferred as the initial value for the target network. Subsequently, the target network is further trained using target domain samples, and the completed training model is saved.
- Step 7: Steps 4~6 are repeated for each value of "n".
- Step 8: The predictive accuracy of each group of models is assessed by the testing set.
- Note: $n = \{10k \mid k \in \mathbb{Z},\ 1 \leq k \leq 21\}$.

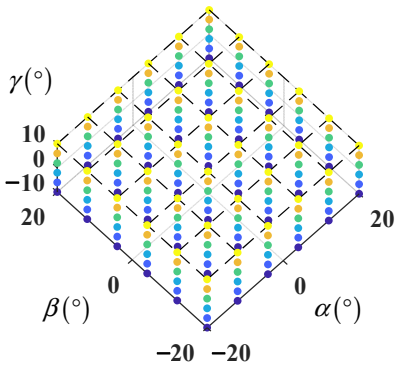

Figure 8. The 216 configurations used to generate data for the target domain.

The conventional BP network also uses a similar set of "n" target domain samples for simulation. Similarly, its training approach only utilizes target domain data to train the initial network structure while keeping the other parameter settings consistent with the transfer network. In other words, 21 models for both the transfer network and the BP network will be trained under 21 different sample numbers of the actual pose. The simulation process for establishing transfer learning models and BP models under different sample numbers of the actual pose is illustrated in Figure 9.

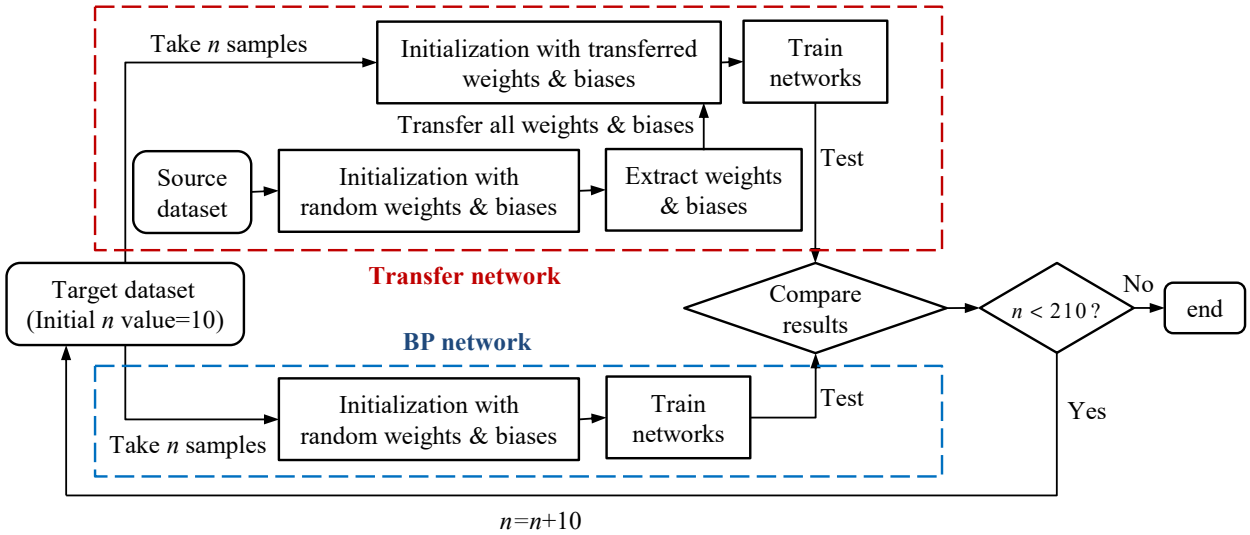

Figure 9. Simulation process for establishing transfer learning models and BP models under different sample numbers of the actual pose.

3.5.2. Simulation Results and Discussion

Following the simulated process described in the preceding section, multiple sets of transfer networks and BP network models are trained by varying the number of actual pose samples. Based on the simulation results, how the sample number of the actual pose obtained in the field of shipborne stabilized platform calibration affects the effectiveness of the transfer learning method is explored. The performance comparison on the testing set of the transfer network and the BP network under varying sample numbers of the actual pose is illustrated in Figure 10.

Each subplot in Figure 10 is divided into three ranges based on the sample number of the actual pose, with the numerical values on the graph indicating the average of the evaluation index for the respective range. It can be observed that transfer learning exhibits varying effects under different sample numbers of the actual pose.

- $10 \leq n < 50$. In this sample range, the transfer networks exhibit a lower average prediction error compared to the BP networks, indicating a notable performance advantage. However, due to the extremely limited number of samples, the predicted accuracy of the networks is constrained. Even for the higher-precision transfer network, the average orientation volumetric error $\|\Delta\boldsymbol{\theta}\|$ after calibration in this range can only be reduced to 1.158°, which is larger than that before calibration of 0.203°. This contradicts the purpose of error compensation. As a result, within this range, neither the transfer network nor the BP network can meet the practical application requirements in marine engineering. They are not acceptable in the field of shipborne stabilized platforms' kinematic calibration.
- $50 \leq n < 180$. In this range, considering each evaluation index, transfer networks continue to demonstrate certain performance advantages over the BP networks. The average $\|\Delta\boldsymbol{\theta}\|$ for transfer networks is 0.364°, smaller than the BP networks' 0.038°. Furthermore, as the sample size increases, the transfer network achieves improved absolute prediction accuracy, notably surpassing the accuracy before calibration. This indicates that not only can the transfer network meet the practical calibration application requirements, but it also exhibits stronger predictive capabilities than the conventional BP network. Thus, transfer learning is the most appropriate approach within this range.
- $180 \leq n \leq 210$. In this range, it can be observed that the lines representing the transfer network and the BP network in the figure closely overlap, indicating no significant difference in their performance. The performance improvement effect of the transfer learning method becomes weak or even non-existent. Therefore, establishing and training a relatively simple BP network is a better choice.

In the entire sample range, the relationship between the effectiveness of transfer learning and the sample number of the actual pose can be summarized as follows: as the number of the actual pose increases, the performance benefit of transfer learning gradually declines and eventually vanishes. Additionally, although different performance advantages of transfer networks are shown at different sample number ranges, transfer learning does not negatively affect the network's performance in any range. This implies that the transfer network has a smaller prediction error when using the same sample number, enhancing calibration accuracy. On the other hand, this suggests that the transfer network requires fewer actual pose samples to achieve the same level of prediction accuracy, saving measurement costs.

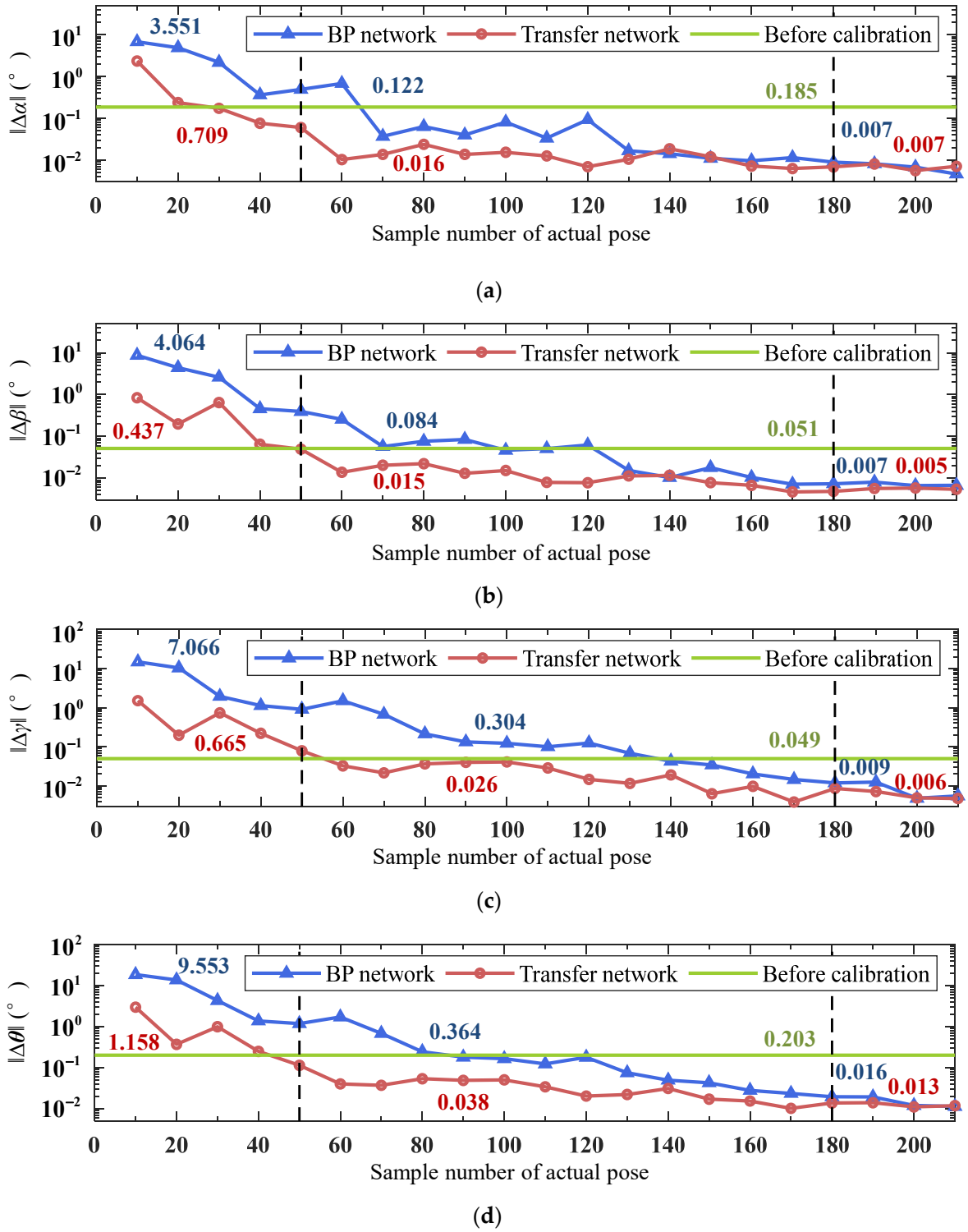

Figure 10. Performance comparison on the testing set of the transfer networks and the BP network under varying sample numbers of the actual pose. (**a**) In the direction of rotation around the *x*-axis; (**b**) in the direction of rotation around the *y*-axis; (**c**) in the direction of rotation around the *z*-axis; (**d**) overall accuracy.

4. Experiments

In this section, stability compensation experiments in a simulated maritime environment were conducted using a 3-UPS/S parallel robot. The effects of attitude compensation

before and after calibration based on the BP network and transfer network are compared to further validate the feasibility and effectiveness of the proposed transfer learning methods.

4.1. Experimental Scheme

The 3-UPS/S parallel stabilized platform is employed as a shipborne stabilized platform to compensate for disturbances caused by the marine environment. Due to the high cost of conducting experiments directly on a ship, the ship simulation platform is used to mimic ship motions induced by factors such as sea waves. The experimental device is shown in Figure 11, with a 3-UPS/S shipborne stabilized platform mounted on top of a ship simulation platform. The ship simulation platform moves according to a predefined command, while the stabilized platform controls the orientation of its moving platform based on the data obtained from the inclinometer, ensuring that the orientation of the moving platform remains horizontal with respect to the ground.

During the operation of the stability compensation experimental system, the inclinometer on the ship simulation platform transmits data to the control system of the stabilized platform. The control system calculates the required compensation attitudes, then employs inverse displacement kinematics to determine the corresponding actuated joint variables, enabling real-time compensation of the stabilized platform. The control strategy for the three actuated limbs is position feedback control based on displacement sensors. Additionally, an inclinometer is installed on the stabilized platform to monitor the compensation effectiveness. The experimental operation diagram is illustrated in Figure 12.

To separately validate the calibration performance of the transfer network and the BP network within the sample range suitable for transfer learning, the accuracies of the end-effector pose trajectory of the stabilized platform before and after offline calibration by embedding both the transfer network and the BP network into the controller are compared. Using the target domain configurations selected in Section 3.4.1 (i.e., Figure 5b, $50 \leq n = 150 < 180$, within the sample range suitable for transfer learning methods) as collected measurement samples, the experimental verification of the stabilized platform attitude compensation effect is conducted. It should be noted that other settings, such as neural network hyperparameters, in the experiment are kept consistent with the simulation.

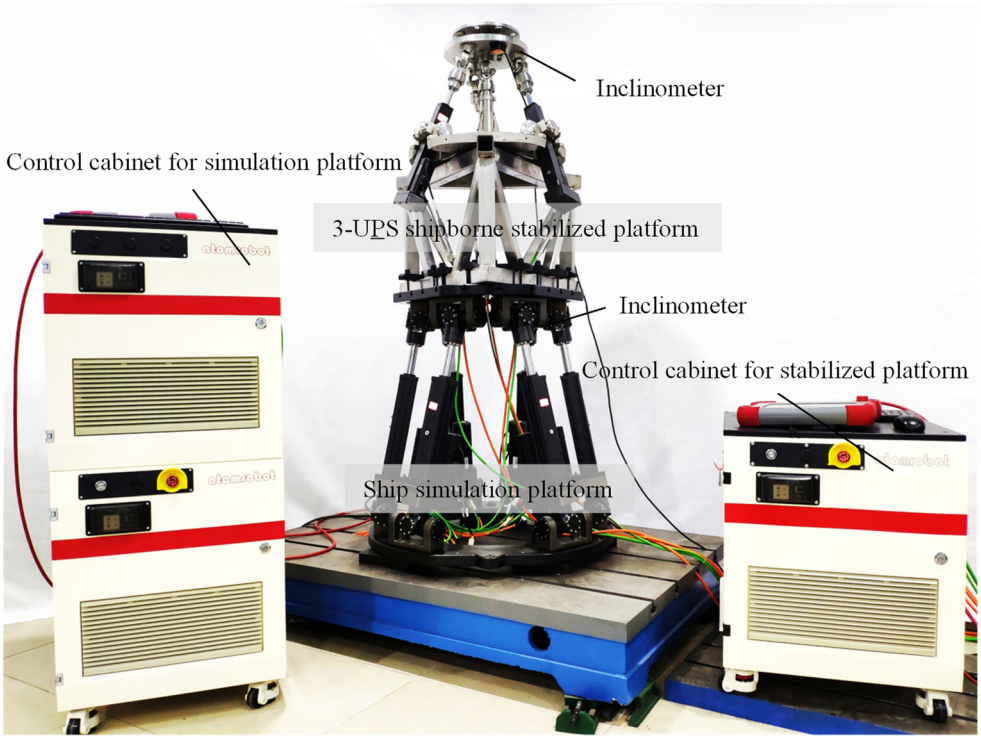

Figure 11. Experimental device.

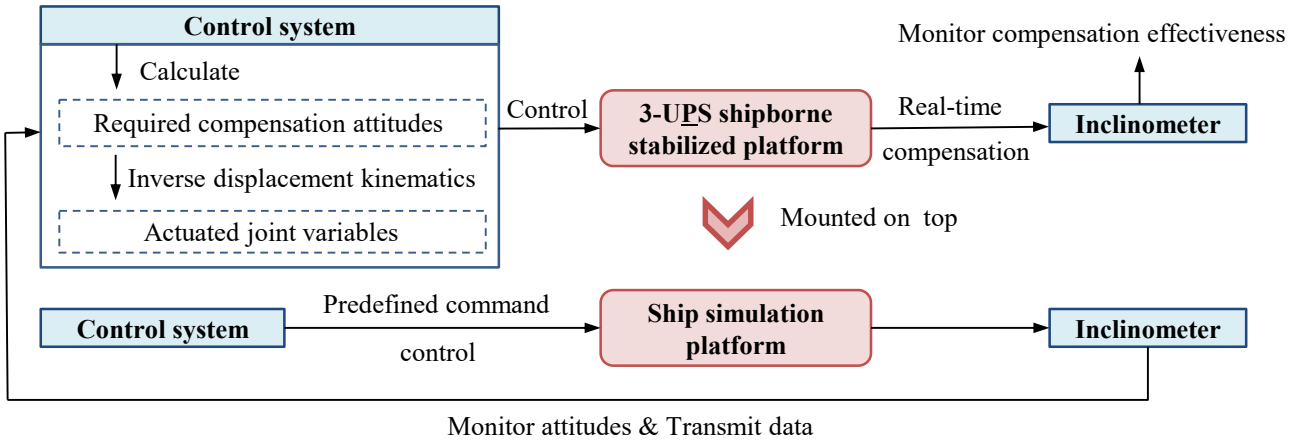

Figure 12. Stability compensation experimental operation diagram.

4.2. Experimental Results and Discussion

The results of the stability compensation experiments based on the transfer network and BP network are presented in Figures 13 and 14 for the training and testing configurations, respectively. It can be observed that although both the BP network and the transfer network effectively reduce end-effector pose errors through calibration, the proposed transfer learning method achieves higher compensation accuracy under the same conditions.

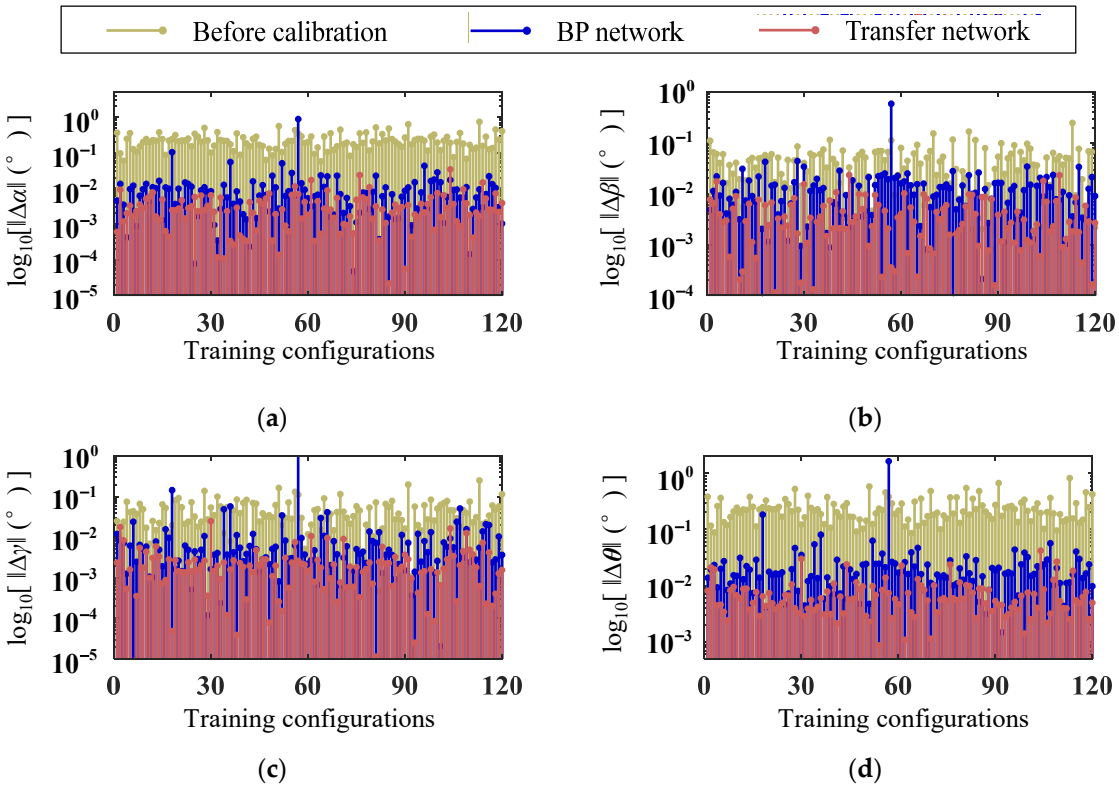

Figure 13. Stability compensation experiment results on the training configurations. (**a**) In the direction of rotation around the *x*-axis; (**b**) in the direction of rotation around the *y*-axis; (**c**) in the direction of rotation around the *z*-axis; (**d**) overall accuracy.

On the testing set, after calibrating the stabilized platform based on the transfer network, the mean orientation error of rotation around the *x*-axis $\|\Delta\alpha\|$ decreases from 0.245° to 0.009°. The mean orientation error of rotation around the *y*-axis $\|\Delta\beta\|$ decreases from 0.051° to 0.006°, and the mean orientation error of rotation around the *z*-axis $\|\Delta\gamma\|$ decreases

from 0.043° to 0.008°. The mean orientation volumetric error $\|\Delta\theta\|$ decreases from 0.257° to 0.017°. In addition, the maximums and standard deviations of the evaluation indices also significantly decrease (see Tables 3 and 4 for details). Figure 15 shows the orientation volumetric errors of the stabilized platform for all configurations before and after kinematic calibration based on the transfer learning method, with the color bar representing the magnitude of the orientation volumetric error. It can be observed that, under these 150 configurations, the stability compensation system achieves the predetermined compensation effect, and the results after compensation are stable with minimal fluctuations. These results demonstrate the superior generalization ability of the transfer network and verify that the proposed method can enhance the accuracy of the 3-UPS/S shipborne stabilized platform and improve the effectiveness of attitude compensation.

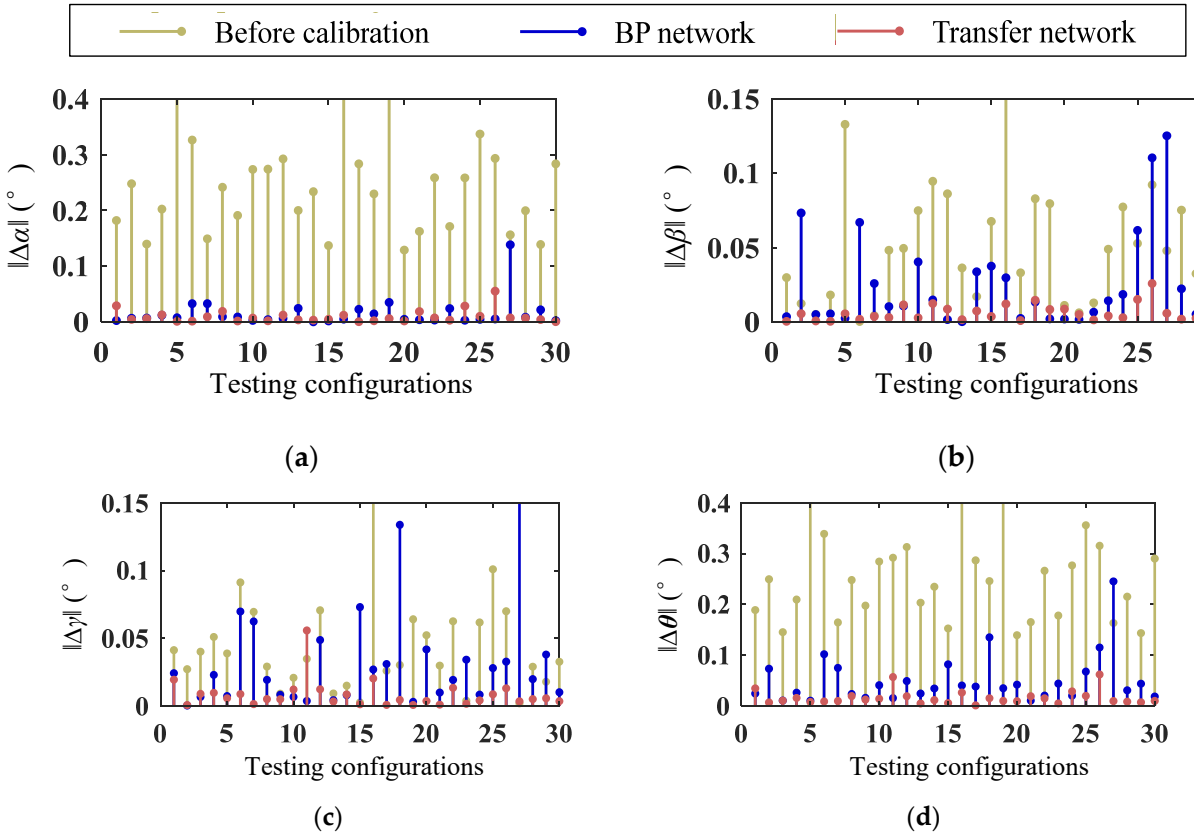

Figure 14. Stability compensation experiment results on the testing configurations. (**a**) In the direction of rotation around the *x*-axis; (**b**) In the direction of rotation around the *y*-axis; (**c**) In the direction of rotation around the *z*-axis; (**d**) Overall accuracy.

Table 3. Experimental comparison of orientation errors for each individual orientation direction on testing configurations.

	Before Calibration			**BP Network**			**Transfer Network**		
	$\|\Delta\alpha\|$	$\|\Delta\beta\|$	$\|\Delta\gamma\|$	$\|\Delta\alpha\|$	$\|\Delta\beta\|$	$\|\Delta\gamma\|$	$\|\Delta\alpha\|$	$\|\Delta\beta\|$	$\|\Delta\gamma\|$
Mean (°)	0.245	0.051	0.043	0.015	0.025	0.032	0.009	0.006	0.008
Maximum (°)	0.495	0.150	0.151	0.138	0.125	0.159	0.055	0.026	0.056
SD (°)	0.093	0.038	0.033	0.025	0.032	0.037	0.011	0.006	0.010

Table 4. Experimental comparison of orientation volumetric error $\|\Delta\theta\|$ on testing configurations.

	Before Calibration	BP Network	Transfer Network
Mean (°)	0.257	0.051	0.017
Maximum (°)	0.506	0.245	0.062
SD (°)	0.090	0.049	0.014

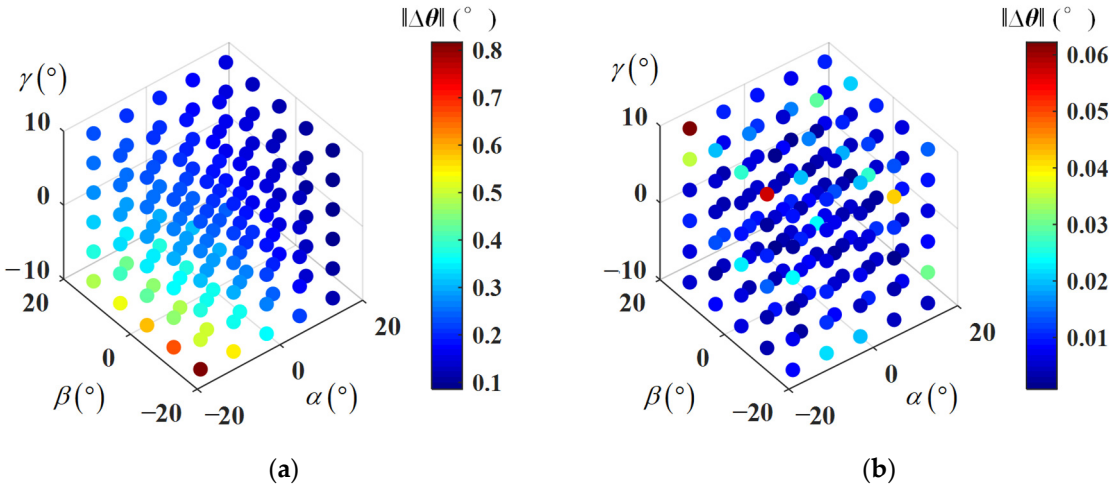

Figure 15. Orientation volumetric errors of the stabilized platform for all configurations. (**a**) Before calibration. (**b**) After calibration based on the transfer learning method.

5. Conclusions

In this study, a kinematic calibration method for the shipborne stabilized platform based on transfer learning was proposed, providing new technological insights to solve the low accuracy problem of conventional neural networks in approximating small-sample measured configurations. The conclusions are as follows:

- A kinematic calibration method for the 3-UPS/S shipborne stabilized platform based on transfer learning was proposed. The method takes "building a mapping model from nominal actuated joint variables to desired end-effector poses" as the source task and "building a mapping model from nominal actuated joint variables to actual end-effector poses" as the target task. Compared with the conventional BP neural network, the method can fully explore and utilize the kinematic information of ideal robot systems. It not only effectively solves the problem of low accuracy when approximating small-sample datasets, but also greatly reduces calibration costs and improves calibration efficiency.
- The impact of the sample number of the actual pose on the effectiveness of transfer learning was investigated. By constructing multiple sets of transfer network models and BP network models under varying sample numbers of the actual pose, the impact pattern was generalized to be that "as the number of the actual pose increases, the performance benefit of transfer learning gradually declines and eventually vanishes." Furthermore, the research range of actual pose sample sizes was quantitatively categorized into three scenarios, and optimal kinematic calibration methods were recommended for each, providing valuable ocean engineering guidance.
- Stability compensation experiments were conducted in a simulated maritime environment. After kinematic calibration based on the transfer learning method, the average orientation volumetric error of the 3-UPS/S robot decreased from 0.257° to 0.017°, representing a 93.4% improvement in accuracy, which is significantly better than the calibration effect achieved by the BP network. The experimental results demon-

strate that kinematic calibration based on transfer learning substantially enhances the end-effector accuracy of the shipborne stabilized platform.

To further advance research on kinematic calibration for shipborne stabilized platforms based on transfer learning, it is essential to consider a more comprehensive range of factors influencing transfer learning, such as the quantity of pre-training data. Furthermore, conducting research on shipborne stabilized platforms with different degrees of freedom to explore the generalizability of this method is also a key focus for future research.

Author Contributions: Conceptualization, M.X. and W.T.; methodology, M.X.; software, M.X. and X.Z.; validation, M.X., W.T. and X.Z.; formal analysis, M.X.; investigation, X.Z.; resources, W.T.; data curation, M.X.; writing—original draft preparation, M.X.; writing—review and editing, M.X., W.T. and X.Z.; visualization, M.X.; supervision, W.T. and X.Z.; project administration, W.T.; funding acquisition, W.T. All authors have read and agreed to the published version of the manuscript.

Funding: This research was funded by the National Key Research and Development Program, grant number 2022YFC3006000.

Institutional Review Board Statement: Not applicable.

Informed Consent Statement: Not applicable.

Data Availability Statement: The datasets generated during and/or analyzed during the current study are available from the corresponding author on reasonable request.

Acknowledgments: The authors would like to thank the funder for supporting them and the Editor and Reviewers for their constructive comments.

Conflicts of Interest: The authors declare no conflicts of interest.

References

1. Liu, Y.; Yuan, H.; Xiao, Z.; Xiao, C. An Offshore Self-Stabilized System Based on Motion Prediction and Compensation Control. *J. Mar. Sci. Eng.* **2023**, *11*, 745. [CrossRef]
2. Qiang, H.; Jin, S.; Feng, X.; Xue, D.; Zhang, L. Model predictive control of a shipborne hydraulic parallel stabilized platform based on ship motion prediction. *IEEE Access* **2020**, *8*, 181880–181892. [CrossRef]
3. Karan, B.; Vukobratović, M. Calibration and accuracy of manipulation robot models—An overview. *Mech. Mach. Theory* **1994**, *29*, 479–500. [CrossRef]
4. Jiang, Y.; Yu, L.; Jia, H.; Zhao, H.; Xia, H. Absolute positioning accuracy improvement in an industrial robot. *Sensors* **2020**, *20*, 4354. [CrossRef] [PubMed]
5. Ma, L.; Bazzoli, P.; Sammons, P.M.; Landers, R.G.; Bristow, D.A. Modeling and calibration of high-order joint-dependent kinematic errors for industrial robots. *Robot. Comput.-Integr. Manuf.* **2018**, *50*, 153–167. [CrossRef]
6. Messay, T.; Messay, R.; Marcil, E. Computationally efficient and robust kinematic calibration methodologies and their application to industrial robots. *Robot. Comput.-Integr. Manuf.* **2016**, *37*, 33–48. [CrossRef]
7. Chen, G.; Kong, L.; Li, Q.; Wang, H.; Lin, Z. Complete, minimal and continuous error models for the kinematic calibration of parallel manipulators based on POE formula. *Mech. Mach. Theory* **2018**, *121*, 844–856. [CrossRef]
8. Tian, W.; Mou, M.; Yang, J.; Yin, F. Kinematic calibration of a 5-DOF hybrid kinematic machine tool by considering the ill-posed identification problem using regularisation method. *Robot. Comput.-Integr. Manuf.* **2019**, *60*, 49–62. [CrossRef]
9. Li, T.; Li, F.; Jiang, Y.; Wng, H. Kinematic calibration of a 3-P(Pa)S parallel-type spindle head considering the thermal error. *Mechatronics* **2017**, *43*, 86–98. [CrossRef]
10. Slamani, M.; Nubiola, A.; Bonev, I.A. Modeling and assessment of the backlash error of an industrial robot. *Robotica* **2012**, *30*, 1167–1175. [CrossRef]
11. Nubiola, A.; Bonev, I.A. Absolute calibration of an ABB IRB 1600 robot using a laser tracker. *Robot. Comput.-Integr. Manuf.* **2013**, *29*, 236–245. [CrossRef]
12. Liu, H.; Yan, Z.; Xiao, J. Pose error prediction and real-time compensation of a 5-DOF hybrid robot. *Mech. Mach. Theory* **2022**, *170*, 104737. [CrossRef]
13. Li, B.; Tian, W.; Zhang, C.; Hua, F.; Cui, G.; Li, Y. Positioning error compensation of an industrial robot using neural networks and experimental study. *Chin. J. Aeronaut.* **2022**, *35*, 346–360. [CrossRef]
14. Gao, G.; Zhang, H.; San, H.; Wu, X.; Wang, W. Modeling and error compensation of robotic articulated arm coordinate measuring machines using BP neural network. *Complexity* **2017**, *2017*, 5156264. [CrossRef]
15. Nguyen, H.N.; Zhou, J.; Kang, H.J. A calibration method for enhancing robot accuracy through integration of an extended Kalman filter algorithm and an artificial neural network. *Neurocomputing* **2015**, *151*, 996–1005. [CrossRef]

16. Yu, D. A new pose accuracy compensation method for parallel manipulators based on hybrid artificial neural network. *Neural. Comput. Appl.* **2021**, *33*, 909–923. [CrossRef]
17. Wang, Y.; Chen, Z.; Zu, H.; Zhang, X.; Mao, C.; Wang, Z. Improvement of heavy load robot positioning accuracy by combining a model-based identification for geometric parameters and an optimized neural network for the compensation of nongeometric errors. *Complexity* **2020**, *2020*, 5896813. [CrossRef]
18. Maghami, A.; Imbert, A.; Côté, G.; Monsarrat, B.; Birglen, L.; Khoshdarregi, M. Calibration of multi-Robot cooperative systems using deep neural networks. *Int. J. Intell. Syst.* **2023**, *107*, 55. [CrossRef]
19. Zhao, G.; Zhang, P.; Ma, G.; Xiao, W. System identification of the nonlinear residual errors of an industrial robot using massive measurements. *Robot. Comput.-Integr. Manuf.* **2019**, *59*, 104–114. [CrossRef]
20. Pan, S.J.; Yang, Q. A survey on transfer learning. *IEEE Trans. Knowl. Data Eng.* **2009**, *22*, 1345–1359. [CrossRef]
21. Zhuang, F.; Qi, Z.; Duan, K.; Xi, D.; Zhu, Y.; Zhu, H.; Xiong, H.; He, Q. A comprehensive survey on transfer learning. *Proc. IEEE Inst. Electr. Electron. Eng.* **2020**, *109*, 43–76. [CrossRef]
22. Venkateswara, H.; Chakraborty, S.; Panchanathan, S. Deep-learning systems for domain adaptation in computer vision: Learning transferable feature representations. *IEEE Signal. Process. Mag.* **2017**, *34*, 117–129. [CrossRef]
23. Yang, B.; Lei, Y.; Li, X.; Roberts, C. Deep targeted transfer learning along designable adaptation trajectory for fault diagnosis across different machines. *IEEE Trans. Ind. Electron.* **2022**, *70*, 9463–9473. [CrossRef]
24. Mosin, V.; Samenko, I.; Kozlovskii, B.; Tikhonov, A.; Yamshchikov, I.P. Fine-tuning transformers: Vocabulary transfer. *Artif. Intell.* **2023**, *317*, 103860. [CrossRef]
25. Yosinski, J.; Clune, J.; Bengio, Y.; Lipson, H. How transferable are features in deep neural networks? *Adv. Neural Inf. Process. Syst.* **2014**, *27*, 3320–3328.
26. Rumelhart, D.E.; Hinton, G.E.; Williams, R.J. Learning representations by back-propagating errors. *Nature* **1986**, *323*, 533–536. [CrossRef]
27. Frank, C.P.; Kevin, M.L. *Modern Robotics: Mechanics, Planning, and Control*; Cambridge University Press: New York, NY, USA, 2017; pp. 68–89.
28. *ISO 230-1*; Test Code for Machine Tools—Part 1: Geometric Accuracy of Machines Operating Under No-Load or Quasi-Static Conditions. International Organization for Standardization: Geneva, Switzerland, 2012.
29. Huang, T.; Zhao, D.; Yin, F.; Tian, W.; Chetwynd, D.G. Kinematic calibration of a 6-DOF hybrid robot by considering multi-collinearity in the identification Jacobian. *Mech. Mach. Theory* **2019**, *131*, 371–384. [CrossRef]
30. *ISO 9283*; Manipulating Industrial Robots—Performance Criteria and Related Test Methods. International Organization for Standardization: Geneva, Switzerland, 1998.
31. Yang, F.; Zhang, W.; Tao, L.; Ma, J. Transfer learning strategies for deep learning-based PHM algorithms. *Appl. Sci.* **2020**, *10*, 2361. [CrossRef]